Beneficial Contribution of Alloy Disorder to Electron and Phonon Transport in Half-Heusler Thermoelectric Materials

*Hanhui Xie, Heng Wang, Yanzhong Pei, Chenguang Fu, Xiaohua Liu, G. Jeffrey Snyder, Xinbing Zhao, and Tiejun Zhu**

Electron and phonon transport characteristics determines the potential of thermoelectric materials for power generation or refrigeration. This work shows that, different from most of high performance thermoelectric materials with dominant acoustic phonon scattering, the promising ZrNiSn based half-Heusler thermoelectric solid solutions exhibit an alloy scattering dominated charge transport. A low deformation potential and a low alloy scattering potential are found for the solid solutions, which is beneficial to maintain a relatively high electron mobility despite of the large effective mass, and can be intrinsic favorable features contributing to the noticeably high power factors of ZrNiSn based alloys. A quantitive description of the different phonon scattering mechanisms suggests that the point defect scattering is the most important mechanism that determines the phonon transport process of the solid solutions. The present results indicate that alloying can be an effective approach for such materials systems to enhance thermoelectric figure of merit *ZT* by reducing phonon thermal conductivity, while minimizing the deterioration of charge mobility due to the low alloy scatteirng potential.

1. Introduction

Thermoelectric (TE) materials, which offer the possibility of directly converting waste heat into usable electricity, could be an important part of the solution to today's energy crisis.[1] The efficiency of a TE material is represented by the dimensionless figure of merit $ZT = \alpha^2\sigma T/\kappa$, where α is the Seebeck coefficient, σ is the electrical conductivity, T is the operating temperature and κ is the total thermal conductivity arising from two prime contributions, namely, the lattice part κ_L and the electronic part κ_e. Two different approaches are often adopted to improve the efficiency of thermoelectrics: increase the power factor ($\alpha^2\sigma$) which is usually achieved by engineering the electronic structure, and reduce κ by introducing additional phonon scattering without the deterioration of power factor.[2] Increased band degeneracy by band convergence,[3–5] resonant states from impurity doping,[5–9] and nanostructure in multiple dimensions[10–15] have been demonstrated to be effective in various systems to achieve high *ZT*.

Further improving *ZT* of TE materials should be based on a better understanding of electron and phonon transport features. The optimal figure of merit *ZT* can be determined by the thermoelectric quality factor $B \propto \mu\, m^{*\,3/2}/\kappa_L$, which is proportional to the density-of-states effective mass m^*, the carriers mobility μ, and the reciprocal lattice thermal conductivity κ_L. The greater quality factor B will lead to the higher *ZT*. According to the deformation potential theory,[16] the mobility interacts with effective mass via $\mu \propto m_I^{*-1} m_b^{*\,-3/2} E^{-2}_{def}$ (m_b^*, the average single valley density-of-states effective mass; m_I^*, the inertial mass of carriers along the conduction direction), when the carriers are scattered by acoustic phonons. The deformation potential E_{def} characterizes the change in energy of the electronic band with elastic deformation and thus describes the coupling between phonons and electrons. A large m^* is favorable to increase α, while it will in turn lead to a significant reduction of mobility.[17] The weak electron-phonon interaction described by a low E_{def} enables the possibility of the coexistence of a high effective mass and a high mobility. However, one can hardly extrapolate the deformation potential to zero.

Forming solid solutions has been considered an effective approach to enhance phonons scattering.[18] Point defect disorder caused by strain and mass differences between alloying atoms and host atoms acts as scattering centers for phonons, which gives rise to the reduction of lattice thermal conductivity κ_L. Meanwhile, the alloy disorder causes local potential energy fluctuation that induces additional carrier scattering leading to a mobility reduction, the strength of which is described by alloy scattering potential E_{al}.[19,20] For most of high performance TE

H. H. Xie, C. G. Fu, X. H. Liu, Prof. X. B. Zhao, Prof. T. J. Zhu
State Key Laboratory of Silicon Materials
Department of Material Science and Engineering
Zhejiang University
Hangzhou 310027, China
Key Laboratory of Advanced Materials and Applications for Batteries of Zhejiang Province
Zhejiang University
Hangzhou 310027, China
E-mail: zhutj@zju.edu.cn
H. Wang, Dr. Y. Pei,[+] Dr. G. J. Snyder
Department of Materials Science
California Institute of Technology
Pasadena, CA 91125, USA
[+]Present address: School of Materials Science and Engineering, Tongji University, 4800 Caoan Road, Shanghai 201804, China

DOI: 10.1002/adfm.201300663

materials and related alloys, the acoustic phonon scattering is dominant for the charge transport.[21–24] Therefore, the E_{def} and E_{al} are the key parameters to characterize the reduction of carrier mobility for TE solid solutions.

Half-Heusler (HH) alloys, with a valence electron count of 18, have been extensively studied as potential high temperature TE materials due to their narrow band gap and sharp slope of the density of states near the Fermi level.[25–30] The HH compounds of the general formula *M*NiSn (*M* = Ti, Hf, Zr) have been of significant interest for their high power factors ($\alpha^2\sigma$) due to the combination of large α and moderate σ. Many efforts have been devoted to tune the carrier concentration by doping Sb on the Sn sites,[25,31] or controlling the atomic antisite disorder.[26,32] To reduce the lattice thermal conducitvity, the effectiveness of isoelectronic alloying on the *M* or Ni sublattice in causing additional mass or strain fluctuation,[25,31,33,34] or grain refinement to enhance phonon scattering at boundaries,[35,36] has been sucessfully demonstrated. A peak value of $ZT \geq 0.8$ has been attained in these compounds,[11,31,34] which meets or exceeds the industry benchmark set by SiGe based high temperature TE alloys.

While the thermoelectric performance of *M*NiSn-based solid solutions has been significantly optimized, few reports have been presented on their electron and phonon transport characteristics. As aforementioned, alloy disorder imposes influences on both electrical and thermal properties, it is imperative to weigh the magnitude of its influence on both the electron and phonon transports. The electronic structure calculations of *M*NiSn compounds performed by different methods[37–40] give similar band configuration that is characterized by single conduction band near Fermi level, which enables the discussion of carrier transport properties using a single parabolic band (SPB) model. The SPB model has been successfully used in various TE materials, like Mo_3Sb_7, La_3Te_4, and $Ba_8Ga_{16}Ge_{30}$ system.[22–24] On the other hand, detailed and accurate study of phonon transport in thermoelectric materials enables better understanding of heat transfer. The method for deducing the relaxation times for phonon scattering processes developed by Callaway,[41] makes it possible to evaluate the contributions from different scattering mechanisms to the total lattice thermal conductivity.

In this paper, we focus on the electron and phonon transport characteristics of high performance HH alloys. Based on the optimized composition of $Hf_{0.65}Zr_{0.35}NiSn_{0.98}Sb_{0.02}$,[31] the Pt substitution at Ni sites is introduced as additional disorder to further reduce the thermal conductivity. The experimental electrical and thermal properties are characterized and modeled. Different from most of typical TE materials, in which the carrier mobility is mainly limited by acoustic phonon scattering,[21–24] the alloy scattering dominated charge transport is found in the HH alloys. A low $E_{al} \approx 0.9$ eV and a low $E_{def} \approx 5$ eV are derived, which compensate for the effect of the large effective mass on the mobility, and can be the intrinsic favorable features contributing to the high power factors of (Hf,Zr)NiSn based alloys. The phonon scattering mechanisms were also quantitively described. The alloying induced point defect scattering, together with Umklapp process, is found to dominate phonon transport process in *M*NiSn(*M* = Ti, Hf, Zr) based HH solid solutions.

2. Results and Discussion

2.1. Electrical Properties and Scattering Potentials

Figure 1 shows the high temperature electrical properties of $Hf_{0.65}Zr_{0.35}Ni_{1-z}Pt_zSn_{0.98}Sb_{0.02}$ (z = 0–0.15) compounds. The electrical conductivity σ and Hall mobility μ_H for all the samples decrease with increasing temperature, indicating a degenerate semiconductor behavior. The Hall carrier concentration n_H exhibits the weak dependence on the Pt substitution ratio, varies from 4.5–6.5 × 10^{20} cm^{-3} and remains nearly constant before intrinsic excitation.The Hall mobility μ_H decreases with the increase of Pt fraction, which may result from the enhanced alloy scattering caused by additional disorder. The μ_H almost exhibits a $T^{-1/2}$ dependence, implying that alloying scattering may be the dominant source of collision.[42] It is noteworthy that the carrier mobility depends less strongly on temperature in degenerate semiconductors, and hence the experimental data of μ_H looks flatter than $T^{-1/2}$.[21] As shown in Figure 1d, the Seebeck coefficient α exhibits the temperature dependence and sign expected for heavily doped n-type semiconductors. Consistent with the behavior of carrier concentration in Figure 1c, the Pt content has no great influence on the α.

The experimental transport data on HH alloys can be analyzed using the common solution to the Boltzmann transport equation within the relaxation time approximation. Assuming that electron conduction occurs within a single parabolic band (SPB), the Seebeck coefficient α and the Hall concentration n_H are given by

$$\alpha = -\frac{k_B}{e}\left(\frac{(2+\lambda)\,F_{\lambda+1}(\eta)}{(1+\lambda)\,F_\lambda(\eta)} - \eta\right) \quad (1)$$

$$n_H = 4\pi\left(\frac{2m^* k_B T}{h^2}\right)^{3/2} F_{1/2} \quad (2)$$

$$F_j(\eta) = \int_0^\infty f\xi^j d\xi \int_0^\infty \frac{\xi^j}{1+e^{(\xi-\eta)}} d\xi \quad (3)$$

Here, k_B, e, h, λ, and m^* are the Boltzmann constant, the electron charge, the Planck constant, the scattering factor and the density-of-state effective mass, respectively. $F_j(\eta)$ is the Fermi integral, described by the reduced chemical potential η defined as $\eta = (E_F - E_c)/(k_B T)$, where E_F is the chemical potential and E_c is the energy of conduction band bottom. It is generally accepted that the acoustic phonon scattering is dominant in limiting the carrier mean free path.[23,24] Luckily, the energy dependence of the relaxation time is the same for acoustic phonon scattering and alloy scattering, both of which give $\lambda = 0$.[43] Thus, the effective mass $m^* \approx 2.9\ m_e$ was obtained at 300 K for $Hf_{0.65}Zr_{0.35}Ni_{1-z}Pt_zSn_{0.98}Sb_{0.02}$ samples, which is in good agreement with the previous reports.[31,44] The calculated temperature dependence of Seebeck coefficient is given in Figure 1d, which deviates from the experimental data above about 500 K, signaturing the onset of the contribution of minor carriers and the invalidity of the SPB model above 500 K.

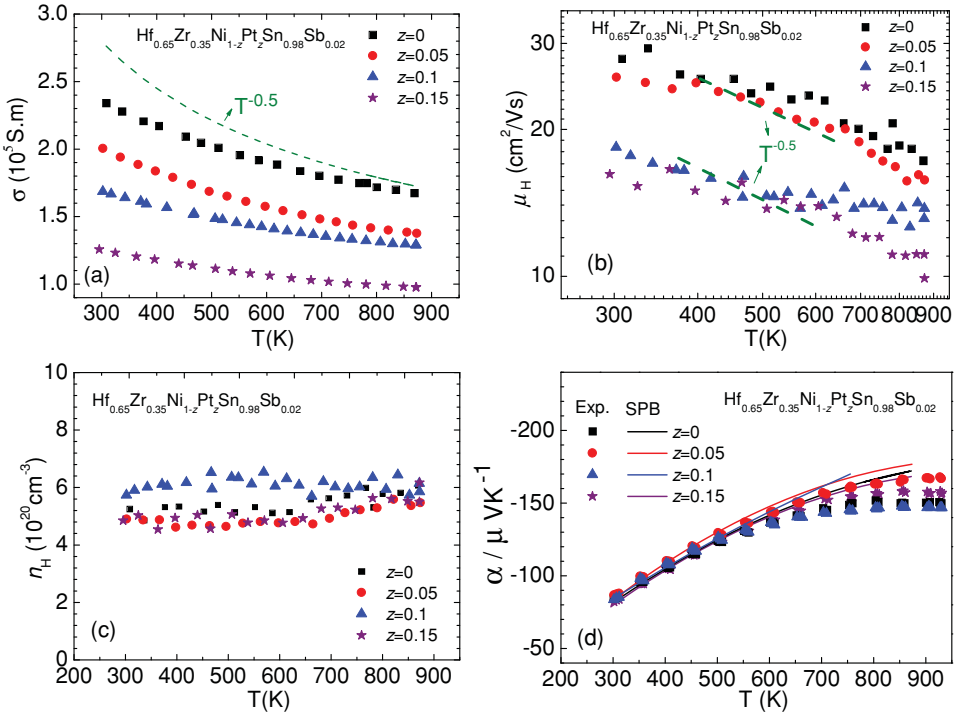

Figure 1. Temperature dependences of a) electrical conductivity σ, b) Hall mobility μ_H, c) carrier concentration n_H, and d) measured and calculated Seebeck coefficient α for $Hf_{0.65}Zr_{0.35}Ni_{1-z}Pt_zSn_{0.98}Sb_{0.02}$ compounds.

The drift mobility μ is related to the Hall mobility μ_H via $\mu_H = \mu\, r_H$, where r_H is the Hall factor. The SPB model with $\lambda = 0$ gives

$$r_H = \frac{3}{2}\frac{F_{1/2}(\eta)\, F_{-1/2}(\eta)}{2F_0^2(\eta)} \tag{4}$$

When the carriers are scattered by both alloy disorder and acoustic phonons, Matthiessen's rule gives an expression for the total μ as $\frac{1}{\mu} = \frac{1}{\mu^{ph}} + \frac{1}{\mu^{al}}$. The deformation potential theory of calculating the scattering by acoustic vibration gives[16,45]

$$\mu^{ph} = \frac{2^{1/2}\pi e\hbar^4}{3(k_B T)^{3/2}} \frac{v_L^2 \rho}{E_{def}^2 \left(m_b^*\right)^{3/2} m_I^*} \frac{F_0(\eta)}{F_{1/2}(\eta)} \tag{5}$$

where v_l is the velocity of longitudinal sound waves, and ρ is the density. The deformation potential E_{def} specifies the strength of the electron-phonon interaction. m_b^* is expressed as $m^* = N_v^{2/3} m_b^*$, where N_v is the number of degenerate carriers pockets. The conduction band extrema for n-type *M*NiSn locates at *X* point of the Brillouin zone, and has three equivalent pockets which dominate the transport properties.[39,40] Harrison and Hauser derived the relaxation time due to scattering in a random alloy,[19] and the drift mobility for alloy scattering can be written as

$$\mu^{al} = \frac{16e\hbar^4}{9\sqrt{2}\pi x(1-x)(k_B T)^{1/2}} \frac{N_0}{E_{al}^2 (m_b^*)^{3/2} m_I^*} \frac{F_0(\eta)}{F_{1/2}(\eta)} \tag{6}$$

where N_0 is the number of atoms per unit volume and x is the fractional concentration. For the case of $Hf_{0.65}Zr_{0.35}Ni_{1-x}Pt_xSn_{0.98}Sb_{0.02}$ compounds, μ^{al} is estimated by the combined scattering from both the Hf-Zr and Pt-Ni disorders, expressed as $\frac{1}{\mu^{al}} = \frac{1}{\mu_{Hf-Zr}} + \frac{1}{\mu_{Pt-Ni}}$. **Figure 2** shows the experimental data and the theoretical calculations for all the samples at 300 K. It explicitly suggests that alloy scattering is the dominant mechanism that limits the Hall mobility, other than the acoustic phonon

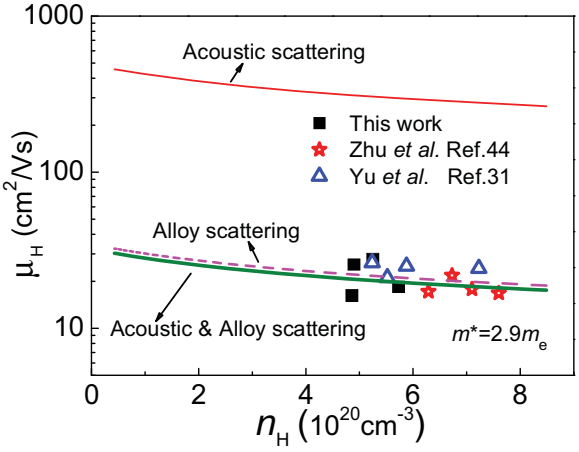

Figure 2. Hall mobility versus carrier concentration for samples from this work at 300 K, as well as data at 300 K from Zhu[44] and Yu[31] et al. The experimental data are compared to theoretical curves calculated by SPB model assuming carrier mobility is limited by acoustic phonon scattering (red solid curve), alloy scattering (pink dash curve), and both of them (green solid curve).The curves were calculated using $m^* = 2.9\ m_e$.

scattering. The values of $E_{al} \approx 0.9$ eV and $E_{def} \approx 5.0$ eV were derived from fitting the experimental mobility data. The typical magnitude of E_{def} is found to be 8–35 eV for semiconductors (Supporting Information, Table S1). The low $E_{def} \approx 5.0$ eV implies the weak interaction between electrons and phonons in this system, which is favorable for a high mobility. $E_{al} \approx 0.9$ eV is reasonable according to the previously reported alloy scattering potential of semiconductors (0.6–2 eV).[18] Compared to $\mu \propto T^{-3/2}$ relationship in an acoustic scattering dominant system, the alloy scattering dominant mechanism gives a relatively weak temperature dependence of mobility via $\mu \propto T^{-1/2}$, which leads to a lower descent rate of mobility, shown in Figure 1b.

It has to be mentioned that ZrNiSn based HH compounds are polar semiconductors due to large electronegativity differences between the constituent elements. Thus the polar optical phonon scattering may play a role in the charge transport. We calculated the Hall mobility due to polar scattering from optical phonons using the polar scattering relaxation time,[21] and found that the polar scattering have appreciable influences on the electron transport at low carrier concentrations below 10^{20} cm^{-3}. At the high carrier concentrations of $n_H \approx 4.5$–6.5×10^{20} cm^{-3} in this work, the contribution of polar scattering to the mobility can be neglected compared to the acoustic phonon scattering, which is well consistent with the recent report on PbS.[46] For the heavily doped TE materials, the screening of polarity vibration by free electrons may take actions.

High ZT can in principle be achieved in a semiconductor with a large value of $\mu m^{*3/2}$. The large effective mass $m^* \approx 2.9 m_e$ of n-type ZrNiSn based HH alloys may result in a low carrier mobility. For comparison, typical TE materials such as PbSe[47] and PbTe,[17] have much larger μ of several hundred cm^2 V^{-1} s^{-1} at room temperature with smaller m^*. However, the present results show that ZrNiSn based solid solutions have the low values of deformation potential and alloy scattering potential, which is beneficial to compensate for the deterioration of mobility caused by the high effective mass. The results also explain why HH alloys have noticeably high power factors among the advanced TE materials. Furthermore, unlike other advanced TE materials with strong acoustic phonon scattering,[21–24] the HH system exhibits an alloy scattering dominant carrier transport, which can be another unique feature for the promising high temperature TE materials.

The Pisarenko plot of α versus n_H from this study and the literature is shown in **Figure 3**, together with the theoretical curves calculated using SPB model with $m^* = 2.9 m_e$ at 300 K and 450 K. The agreement between calculations and experiment strongly justifies the use of SPB model for the analysis of electronic transport in the (Hf,Zr)NiSn system. The trivial change of m^* suggests that the substitution of Pt for Ni has a minor effect on the band structure of the half-Heusler alloys. A temperature-independent effective mass was obtained, which can be understood by an insignificant change of the chemical potential η (from $3k_BT$ at 300 K to $1.5k_BT$ for 500 K) in the edge of the conduction band.

2.2. Phonon Transport and ZT Values

The temperature dependences of total thermal conductivity κ and the lattice thermal conductivity κ_L are plotted in

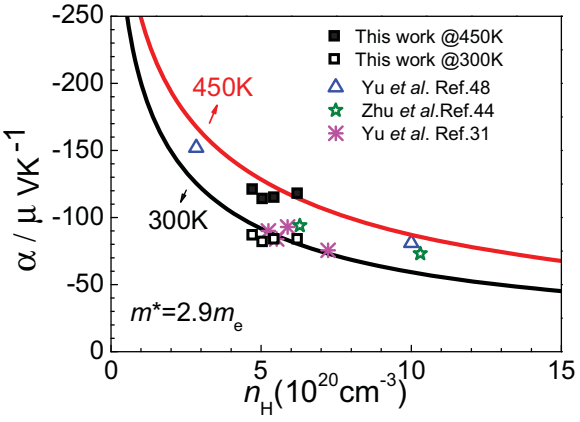

Figure 3. Seebeck coefficient versus the Hall carrier density of $Hf_{0.65}Zr_{0.35}Ni_{1-z}Pt_zSn_{0.98}Sb_{0.02}$ samples at 300 K and 450 K, together with the literature data.[31,44,48]

Figure 4. The total thermal conductivity for all samples declines with increasing temperature before bipolar conduction begins. The lattice thermal conductivity was obtained by subtracting the electronic contribution from the measured κ. The electronic part was calculated via the Wiedemann-Franz relationship, $\kappa_e = L\sigma T$, where L is the Lorenz number and can be calculated with the expression

$$L = -\frac{k_B^2}{e^2}\frac{(1+\lambda)(3+\lambda)F_\lambda(\eta)F_{2+\lambda}(\eta) - (2+\lambda)^2 F_{1+\lambda}(\eta)^2}{(1+\lambda)^2 F_\lambda(\eta)^2} \quad (7)$$

The calculated L values decrease with the increase of temperature for all samples (due to decreasing η), as shown in Figure 4b.

The κ_L within the whole measured temperature range decreases with the increase of Pt ratio, mainly resulting from the enhancement of phonon scattering, but still much higher than the theoretical minimum lattice thermal conductivity, $\kappa_{L_{min}}$ calculated by Cahill's formulation.[49] The lattice thermal conductivity displayed a $\kappa_L \propto T^{-1/2}$ relationship, as shown in Figure 4d, indicating the existence of strong alloy scattering of phonons.[50]

The complex interplay of phonon scattering can be estimated by the Callaway model based on relaxation times approximation, assuming that there is no phonon dispersion and the longitudinal and transverse polarizations behave identically.[51] A simplified version of Callaway model gives Equation 8, which neglect the small correction term for Normal phonon-phonon interaction.[41]

$$\kappa = \frac{k_B}{2\pi^2 v}\left(\frac{k_B}{\hbar}\right)^3 T^3 \int_0^{\theta_D/T} \tau(x)\frac{x^4 e^x}{(e^x-1)^2}dx \quad (8)$$

Here, x is defined as $x = \hbar\varpi/k_BT$ (ω is the phonon frequency), v is the phonon velocity and θ_D is the Debye temperature. Debye model gives the relationship between Debye temperature θ_D and Debye frequency ω_D as $k_B\theta_D = \varpi_D$.The Debye temperature is calculated from the measured longitudinal and transverse sound velocities, v_l and v_t, and atom number in a unit volume n via $v = \left\{\frac{1}{3}\left(\frac{1}{v_l^3} + \frac{2}{v_t^3}\right)\right\}^{-1/3}$ and $\theta_D = v(6\pi^2 n)^{1/3}/k_B$.

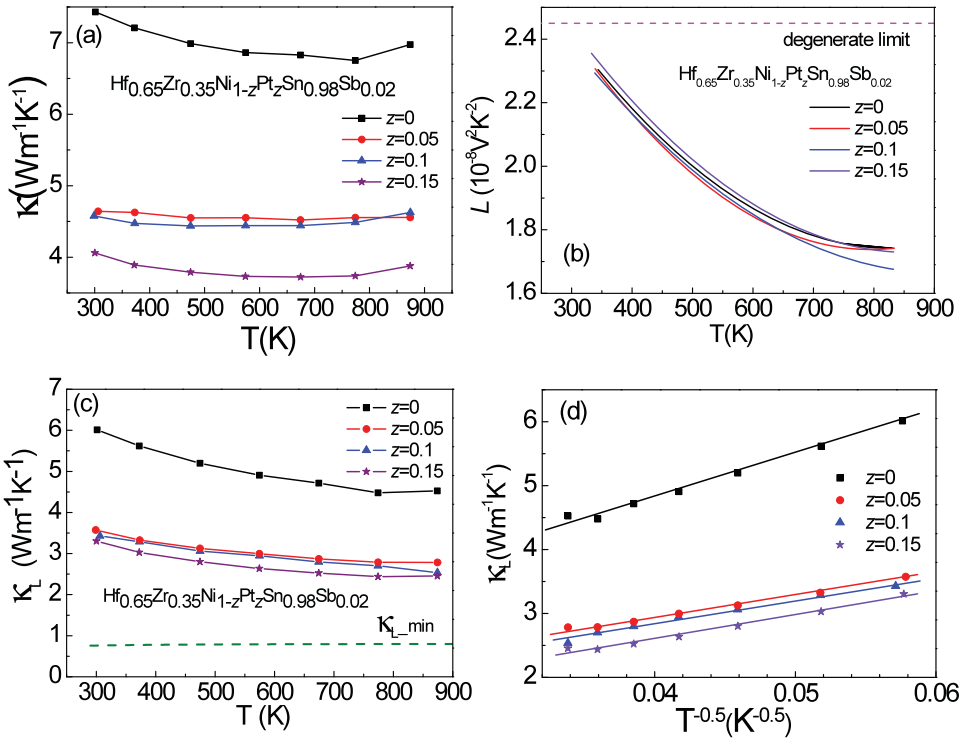

Figure 4. Temperature dependences of a) total thermal conductivity κ, b) the Lorenz number, c) the lattice thermal conductivity κ_L, and d) the lattice thermal conductivity κ_L versus $T^{-0.5}$, for $Hf_{0.65}Zr_{0.35}Ni_{1-z}Pt_zSn_{0.98}Sb_{0.02}$.

Thermal conductivity is typically limited by phonon-phonon scattering, phonon-electron scattering, point defect scattering, and boundary scattering. With the basic assumption of Matthiessen's rule[52] the combined relaxation time τ_C can be obtained by the addition of the inverse relaxation times for the different scattering processes, $\tau_c^{-1} = \sum_i \tau_i^{-1}$, where τ_i refers to the phonon relaxation time for the ith scattering process.

At temperatures in the region of $T \geq 0.1\ \theta_D$, the Umklapp scattering is believed to be crucially important.[53] An empirical expression of τ_U described by the Grueneisen parameter γ, volume per atom V, and the average mass M gives:

$$\tau_U^{-1} = \frac{\hbar\gamma^2\varpi^2 T}{Mv^2\theta_D}\exp\left(-\frac{\theta_D}{3T}\right) \quad (9)$$

Grueneisen parameter, which strongly depends on the anharmonicity of the bonding, is given as $\gamma = \frac{3\beta B_m V_m}{C_v}$, where β, V_m, B_m, C_v are linear thermal expansion coefficient, the molar volume, isothermal bulk modulus, and heat capacity. Isothermal bulk modulus B_m can be estimated from the measured transverse sound velocity v_t and density ρ, via $v_t = \sqrt{B_m/\rho}$.

Scattering by point defects arises from both mass and strain differences within the lattice. In the simple case of alloying, τ_{PD} is given by

$$\tau_{PD}^{-1} = \tau_M^{-1} + \tau_S^{-1} = \frac{V\varpi^4}{4\pi v^3}(\Gamma_M + \Gamma_S) \quad (10)$$

where Γ_M and Γ_S are the disorder scattering parameters due to mass and strain field fluctuations, respectively. Yang et al. have successfully demonstrated the use of the disorder scattering parameters in calculating the point defect scattering in ZrNiSn-based HH alloys.[54]

Ziman obtained an expression of the phonon relaxation time for scattering by free electrons in a parabolic model.[55] At high carrier concentrations,[56] the derivation is given as:

$$\tau_{pe}^{-1} = \frac{E_{def}^2 m^{*2}\varpi}{2\pi\hbar^3\rho v_1} \quad (11)$$

Boundary scattering in polycrystalline materials with grain size d can be estimated from $\tau_B = \frac{d}{v}$.[57] The effect of boundary scattering may be important in non-single crystal materials or in very thin film. Sintered materials show this effect particularly strongly.[56] In this paper, d = 1.5 μm was estimated from the scanning electronic microscopy observation (Supporting Information, Figure S1), which is similar with our previous results.[31,42,48,58]

The parameters used for calculations are shown in **Table 1**. The linear thermal expansion coefficient β is about 12.1×10^{-6} K^{-1} based on the thermal expansion measurement of ZrNiSn.[59]

The scattering mechanisms discussed above target different populations of phonons, as shown in **Figure 5**a. The curves are calculated at 400 K, when all of the vibration modes have been excited and the maximum phonon frequency is the Debye frequency. It is generally accepted that Umklapp and point defect scattering target high frequency phonons, while the boundary scattering is often the dominant mechanism at low frequencies.[51] In this work, $\tau_{PD} \approx 6 \times 10^{-14}$ s at Debye frequency were obtained for $Hf_{0.65}Zr_{0.35}Ni_{0.85}Pt_{0.15}Sn_{0.98}Sb_{0.02}$ sample, implying

Table 1. Room-temperature sound velocities by ultrasonic measurement and calculated parameters for $Hf_{0.65}Zr_{0.35}Ni_{1-z}Pt_zSn_{0.98}Sb_{0.02}$ samples.

Pt ratio	v_l [m s^{-1}]	v_t [m s^{-1}]	v [m s^{-1}]	Young's Modulus [Gpa]	θ_D	γ
0	4953	2927	3242	199	366	0.92
0.05	4956	2923	3238	198	361	0.91
0.1	4908	2917	3229	196	360	0.90
0.15	4800	2842	3147	190	350	0.86

that strong point defect scattering exists, which is consistent with the results shown in Figure 4d. In combination, these scattering mechanisms lead to an effective τ that envolves in the calculations of the lattice thermal conductivity.

The comparison of experimental and theoretical lattice thermal conducitivities for $Hf_{0.65}Zr_{0.35}Ni_{1-z}Pt_zSn_{0.98}Sb_{0.02}$ is shown in Figure 5b. The target temperature is 400 K, when all the vibration modes have been excited and bipolar conduction has not yet begun. The point defect scattering is the dominant source of collisions, which sets an limit to the lattice thermal

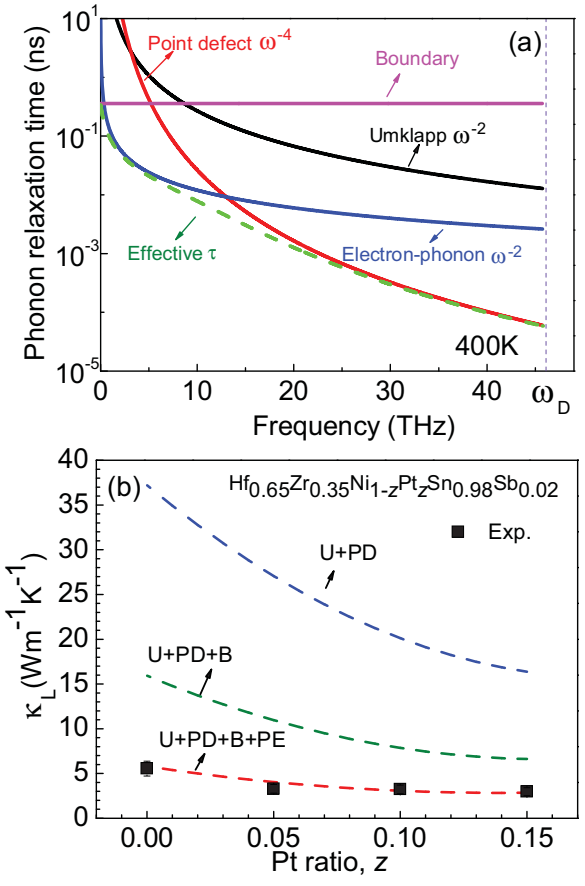

Figure 5. a) Calculated phonon relaxation time τ versus frequency ω at 400 K for $Hf_{0.65}Zr_{0.35}Ni_{0.85}Pt_{0.15}Sn_{0.98}Sb_{0.02}$ sample. b) Comparison of experimental and calculated lattice thermal conducitivities at 400 K for $Hf_{0.65}Zr_{0.35}Ni_{1-z}Pt_zSn_{0.98}Sb_{0.02}$.

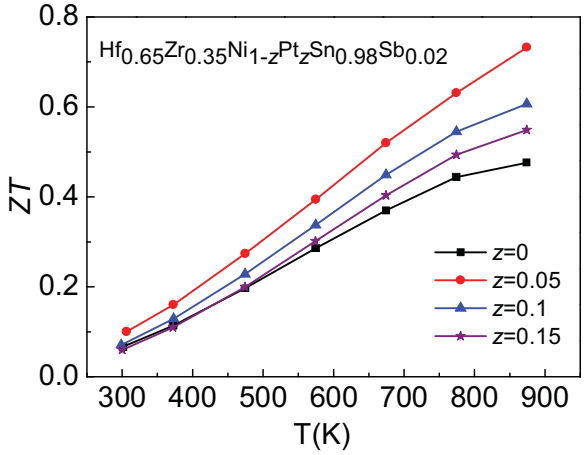

Figure 6. Temperature dependence of the dimensionless figure of merit ZT for $Hf_{0.65}Zr_{0.35}Ni_{1-z}Pt_zSn_{0.98}Sb_{0.02}$.

conductivity. Electron-phonon scattering, which is often believed as low temperature effect, may become an important part in semiconductors with high carrier concentrations, especially for systems with a large effective mass. It is reported that electron-phonon coupling contributes significantly to the reduction of lattice thermal conductivity in heavily doped n-type $CoSb_3$.[60,61] With high carrier concentration $n \approx 5–6 \times 10^{20}$ cm^{-3} as well as large effective mass $m^* \approx 2.9m_e$, phonon-electron interactions forms an unnegligible part of scattering in doped n-type ZrNiSn based alloys. Boundary scattering, though believed to be negligible at high temperatures in some systems,[22] proves to be important in sintered HH alloys with small grain sizes as shown in Figure 5b, which is consistent with previous reports.[35,36,62] The calculated κ_L considering all these scattering mechanisms matches well with the experimental values, indicating that calculations based on Callaway model can give a prediction to the thermal conductivity for HH system. The calculated spectral thermal conductivity k_s also supports the above discussions (Suppoting Information, Figure S2).

The high temperature figure of merit ZT was calculated and shown in **Figure 6**. All the Pt substituted samples exhibit an improvement of ZT compared to the parent compound, implying that the alloy disorder is beneficial for high performance of the alloy system, especially at high temperatures. The highest ZT value reaches ≈0.75 at 875 K for $Hf_{0.65}Zr_{0.35}Ni_{0.95}Pt_{0.05}Sn_{0.98}Sb_{0.02}$, comparable to the state-of-the-art value of ZT≈0.8.[11,31,34] The higher ZT can be desirable with further increasing temperature.

3. Conclusions

The thermoelectric transport of Pt substituted (Hf,Zr)NiSn-based HH solid solutions were systematically investigated. The strong alloy scattering was found in this system, in addition to the acoustic phonon scattering that is the most important scattering mechanism in most of advanced TE materials. A low deformation potential and a low alloy scattering potential were

derived, which are beneficial to compensate for the decrease of mobility due to the large effective mass, and also contribute to high power factors in n-type ZrNiSn-based half-Heusler system. The Callaway formalism for the phonon relaxation times was adopted to distinguish the different scattering mechanisms, and the results suggest that strong point defect scattering exists in phonon transport, which is consistent with the experimental $\kappa_L \approx T^{-0.5}$ relationship. Pt substitution on Ni site is proved effective in suppressing thermal conductivity by ≈40% reduction at 870 K. The present work indicates that alloying can be an effective approach for such materials systems to enhance the thermoelectric figure of merit ZT by enhancing point defect phonon scattering, while minimizing the deterioration of charge mobility due to the low alloy scattering potential.

4. Experimental Section

The high purity of samples were fabricated by a time-efficient method combining levitation melting and spark plasma sintering (SPS).[31,44] Alloys with nominal composition $Hf_{0.65}Zr_{0.35}Ni_{1-z}Pt_zSn_{0.98}Sb_{0.02}$ (z = 0, 0.05, 0.1, 0.15) were first prepared by levitation melting of stoichiometric amounts of Hf (piece, 99.99%), Zr (piece, 99.99%), Ni (block, 99.999%), Pt (particles, 99.999%), Sn (particles, 99.999%), and Sb (block, 99.99%) under an argon atmosphere for 2 min, and the melt was quenched in a water-cooled copper crucible. The ingots were remelted twice to ensure homogeneity. Mechanical milling was carried out with normal butane protection at 200 rpm for 4 h. The powders were then sintered by SPS (SPS-1050, Sumitomo Coal Mining Co.) at 1175 K under 65 MPa in vacuum for 10 min. The as-sintered samples, of which the relative density was found to be ≈95%, were used for measurements of thermal conductivity and Hall data, and then cut into rectangular bars for Seebeck coefficient and electrical conductivity measurements.

The phase structure of the powders and sintered samples were studied by X-ray diffraction (XRD) on a RigakuD/MAX-2550PC diffractometer using Cu K_a radiation (λ = 1.5406 Å) and the chemical composition was obtained during electron probe microanalysis (EPMA, JOEL, JXA-8100) using wavelength dispersive spectroscopy (WDS). The XRD patterns of all samples could be indexed to the *M*NiSn based half-Heusler phase with a cubic MgAgAs-type crystal structure (Supporting Information, Figure S3). The EPMA results revealed that the compositions of the $Hf_{0.65}Zr_{0.35}Ni_{1-z}Pt_zSn_{0.98}Sb_{0.02}$ (z = 0, 0.05, 0.1, 0.15) samples were very close to the nominal ones (Supporting Information, Table S2). The electrical transport was characterized via Hall effect, electrical conductivity, and Seebeck coefficient measurements. The in-plane electrical resistivities and Hall coefficients were measured using the Van der Pauw method in a magnetic field up to ±2 T. The Hall carrier concentration n_H is calculated via $n_H = 1/eR_H$, where R_H is the Hall coefficient and e is the electron charge. The Hall mobility μ_H is calculated from the Hall coefficient and electrical conductivity $\mu_H = R_H\sigma$. The electrical conductivity and Seebeck coefficient from 300–900 K were measured on a commercial Linseis LSR-3 system using a DC four-probe method and differential voltage/temperature technique, respectively. The thermal conductivity κ was calculated by using $\kappa = D\rho C_p$, where ρ is the sample density estimated by an Archimedes' method. The thermal diffusivity D, and specific heat C_p, were measured by a laser flash method on Netzsch LFA457 instrument with a Pyroceram standard.

Normal and shear ultrasonic measurements were performed at room temperature using input from a Panametrics 5052 pulser/receiver with the filter at 0.03 MHz. The response was recorded via a Tektronic TDS5054B-NV digital oscilloscope. The high-resolution mode was employed for the longitudinal speed of sound and an averaging mode (16 wave forms) was utilized for the transverse speed-of-sound measurements.

Supporting Information

Supporting Information is available from the Wiley Online Library or from the author.

Acknowledgements

The authors would like to thank Prof. Jihui Yang from the University of Washington, Seattle for the valuable discussions. This work is supported by the National Basic Research Program of China (Grant No.2013CB632503), the Nature Science Foundation of China (Grant Nos.51171171 and 51271165), and the Program for New Century Excellent Talents in University (NCET-12-0495). Y.P. acknowledges the National Junior 1000 Plan and Shanghai Eastern Scholar program for funding supports.

Received: February 21, 2013
Revised: March 18, 2013
Published online: April 30, 2013

[1] T. M. Tritt, *Science* **1999**, *283*, 804.
[2] G. J. Snyder, E. S. Toberer, *Nat. Mater.* **2008**, *7*, 105.
[3] Y. Pei, X. Shi, A. LaLonde, H. Wang, L. Chen, G. J. Snyder, *Nature* **2011**, *473*, 66.
[4] W. Liu, X. Tan, K. Yin, H. Liu, X. Tang, J. Shi, Q. Zhang, C. Uher, *Phys. Rev. Lett.* **2012**, *108*, 166601.
[5] Y. Pei, H. Wang, G. J. Snyder, *Adv. Mater.* **2012**, *24*, 6125.
[6] C. M. Jaworski, B. Wiendlocha, V. Jovovica, J. P. Heremans, *Energy Environ. Sci.* **2011**, *4*, 4155.
[7] J. P. Heremans, B. Wiendloch, A. M. Chamoire, *Energy Environ. Sci.* **2012**, *5*, 5510.
[8] Q. Zhang, H. Wang, W. Liu, H. Wang, B. Yu, Q. Zhang, Z. Tian, G. Ni, S. Lee, K. Esfarjani, G. Chen, Z. Ren, *Energy Environ. Sci.* **2012**, *5*, 5246.
[9] J. P. Heremans, V. Jovovic, E. S. Toberer, A. Saramat, K. Kurosaki, A. Charoenphakdee, S. Yamanaka, G. J. Snyder, *Science* **2008**, *321*, 554.
[10] H. Lu, P. G. Burke, A. C. Gossard, G. Zeng, A. T. Ramu, J. Bahk, J. E. Bowers, *Adv. Mater.* **2011**, *23*, 2377.
[11] G. Joshi, X. Yan, H. Wang, W. Liu, G. Chen, Z. F. Ren, *Adv. Energy Mater.* **2011**, *1*, 643.
[12] X. Yan, G. Joshi, W. Liu, Y. Lan, H. Wang, S. P. Lee, J. W. Simonson, S. J. Poon, T. M. Tritt, G. Chen, Z. F. Ren, *Nano Lett.* **2011**, *11*, 556.
[13] S. K. Bux, R. G. Blair, P. K. Gogna, H. Lee, G. Chen, M. S. Dresselhaus, R. B. Kaner, J. P. Fleurial, *Adv. Funct. Mater.* **2009**, *19*, 2445.
[14] C. J. Vineis, A. Shakouri, A. Majumdar, M. G. Kanatzidis, *Adv. Mater.* **2010**, *22*, 3970.
[15] A. J. Minnich, M. S. Dresselhaus, Z. F. Ren, G. Chen, *Energy Environ. Sci.* **2009**, *2*, 466.
[16] J. Bardeen, W. Shockley, *Phys. Rev.* **1950**, *80*, 72.
[17] Y. Pei, A. D. LaLonde, H. Wang, G. J. Snyder, *Energy Environ. Sci.* **2012**, *5*, 7963.
[18] H. Wang, A. D. LaLonde, Y. Pei, G. J. Snyder, *Adv. Funct. Mater.* **2013**, *23*, 1586.
[19] J. W. Harrison, J. R. Hauser, *Phys. Rev. B* **1976**, *13*, 5347.
[20] J. W. Harrison, J. R. Hauser, *J. Appl. Phys.* **1976**, *47*, 292.
[21] Y. I. Ravich, B. A. Efimova, I. A. Smirnov, *Semiconducting Lead Chalcogenides*, Plenum press, New York, USA, **1970**.
[22] X. Shi, Y. Pei, G. J. Snyder, L. Chen, *Energy Environ. Sci.* **2011**, *4*, 4086.
[23] A. F. May, E. F. Larsen, G. J. Snyder, *Phys. Rev. B* **2010**, *81*, 125205.

[24] A. F. May, E. S. Toberer, A. Saramat, G. J. Snyder, *Phys. Rev. B* **2009**, *80*, 125205.
[25] C. Uher, J. Yang, S. Hu, D. T. Morelli, G. P. Meisner, *Phys. Rev. B* **1999**, *59*, 8615.
[26] P. Qiu, J. Yang, X. Huang, X. Chen, L. Chen, *Appl. Phys. Lett.* **2010**, *96*, 152105.
[27] S. R. Culp, J. W. Simonson, S. J. Poon, V. Ponnambalam, J. Edwards, T. M. Tritt, *Appl. Phys. Lett.* **2008**, *93*, 022105.
[28] Y. Xia, S. Bhattacharya, V. Ponnambalam, A. L. Pope, S. J. Poon, T. M. Tritt, *J. Appl. Phys.* **2000**, *88*, 1952.
[29] K. Kawano, K. Kurosaki, T. Sekimoto, H. Muta, S. Yamanaka, *Appl. Phys. Lett.* **2007**, *91*, 062115.
[30] J. Yang, H. Li, T. Wu, W. Zhang, L. Chen, J. Yang, *Adv. Funct. Mater.* **2008**, *18*, 2880.
[31] C. Yu, T. J. Zhu, R. Z. Shi, Y. Zhang, X. B. Zhao, J. He, *Acta Mater.* **2009**, *57*, 2757.
[32] H. H. Xie, J. L. Mi, L. P. Hu, N. Lock, M. Chirstensen, C. G. Fu, B. B. Iversen, X. B. Zhao, T. J. Zhu, *CrystEngComm* **2012**, *14*, 4467.
[33] X. Yan, W. Liu, H. Wang, S. Chen, J. Shiomi, K. Esfarjani, H. Wang, D. Wang, G. Chen, Z. F. Ren, *Energy Environ. Sci.* **2012**, *5*, 7543.
[34] P. J. Lee, L. S. Chao, *J. Alloys Compd.* **2010**, *504*, 192.
[35] S. Bhattacharya, M. J. Skove, M. Russell, T. M. Tritt, *Phys. Rev. B* **2008**, *77*, 184203.
[36] S. Bhattacharya, T. M. Tritt, Y. Xia, V. Ponnambalam, S. J. Poon, N. Thadhani, *Appl. Phys. Lett.* **2002**, *81*, 43.
[37] S. Ouardi, G. H. Fecher, B. Balke, X. Kozina, G. Stryganyuk, C. Felser, *Phys. Rev. B* **2010**, *82*, 085108.
[38] S. Ogut, K. M. Rabe, *Phys. Rev. B* **1995**, *51*, 10443.
[39] P. Larson, S. D. Mahanti, M. G. Kanatzidis, *Phys. Rev. B* **2000**, *62*, 12754.
[40] L. Chaput, J. Tobola, P. Pécheur, H. Scherrer, *Phys. Rev. B* **2006**, *73*, 045121.
[41] J. Callaway, *Phys. Rev.* **1959**, *113*, 1046.
[42] K. Srinivasan, A. Sher, C. An-Ban, *Appl. Phys. Lett.* **1985**, *47*, 160.
[43] V. I. Fistul, *Heavily Doped Semiconductors*, Plenum press, New York, USA **1969**.
[44] T. J. Zhu, K. Xiao, C. Yu, J. J. Shen, S. H. Yang, A. J. Zhou, X. B. Zhao, J. He, *J. Appl. Phys.* **2010**, *108*, 044903.
[45] H. J. Goldsmid, *Thermoelectric refrigeration*, Plenum Press, New York, USA **1964**.
[46] H. Wang, E. Schechtel, Y. Pei, G. J. Snyder, *Adv. Energy Mater.* **2012**, *3*, 488.
[47] H. Wang, Y. Pei, A. D. LaLonde, G. J. Snyder, *Proc. Natl. Acad. Sci. USA* **2012**, *109*, 9705.
[48] C. Yu, T. J. Zhu, K. Xiao, J. J. Shen, S. H. Yang, X. B. Zhao, *J. Electron. Mater.* **2010**, *39*, 2008.
[49] D. G. Cahill, S. K. Watson, R. O. Pohl, *Phys. Rev. B* **1992**, *46*, 6131.
[50] P. G. Klemens, *Phys. Rev.* **1960**, *119*, 507.
[51] C. M. Bhandari, D. M. Rowe, *Thermal conduction in semiconductors*, Wiley Eastern Limited, New Delhi, India **1988**.
[52] N. W. Ashcroft, N. D. Mermin, *Solid State Physics* Thomson Learning, New York **1976**.
[53] G. A. Slack, S. Galginaitis, *Phys. Rev.* **1964**, *133*, A253.
[54] J. Yang, G. P. Meisner, L. Chen, *Appl. Phys. Lett.* **2004**, *85*, 1140.
[55] J. M. Ziman, *Philos. Mag.* **1956**, *1*, 191.
[56] J. E. Parrott, *Rev. Int. Hautes Temp. Refract.* **1979**, *16*, 393.
[57] H. J. Goldsmid, A. W. Penn, *Phys. Lett. A* **1968**, *A27*, 523.
[58] H. H. Xie, C. Yu, T. J. Zhu, C. G. Fu, G. J. Snyder, X. B. Zhao, *Appl. Phys. Lett.* **2012**, *100*, 254104.
[59] D. Y. Jung, K. Kurosaki, C. E. Kima, H. Muta, S. Yamanaka, *J. Alloys Compd.* **2010**, *489*, 328.
[60] H. Anno, K. Matsubara, Y. Notohara, T. Sakakibara, H. Tashiro, *J. Appl. Phys.* **1999**, *86*, 3780.
[61] J. Yang, D. T. Morelli, G. P. Meisner, W. Chen, J. S. Dyck, C. Uher, *Phys. Rev. B* **2002**, *65*, 094115.
[62] C. Yu, T. J. Zhu, K. Xiao, J. J. Shen, X. B. Zhao, *Funct. Mater. Lett.* **2010**, *3*, 227.